ELSEVIER

Journal of Nuclear Materials 258–263 (1998) 85–96

journal of nuclear materials

Materials design data for fusion reactors

A.A.F. Tavassoli *

CEREM, Commissariat à l'Energie Atomique, CEA/Saclay, 91191 Gif sur Yvette CEDEX, France

Abstract

Design data needed for fusion reactors are characterized by the diversity of materials and the complexity of loading situations found in these reactors. In addition, advanced fabrication techniques, such as Hot Isostatic Pressing, envisaged for fabrication of single and multilayered in-vessel components, could significantly change the original materials properties for which the current design rules are written. As a result, additional materials properties have had to be generated for fusion reactors and new structural design rules formulated. This paper recalls some of the materials properties data generated for ITER and DEMO, and gives examples of how these are converted into design criteria. In particular, it gives specific examples for the properties of 316LN-IG and Modified 9Cr–1Mo steels, and CuCrZr alloy. These include, determination of tension, creep, isochronous, fatigue, and creep–fatigue curves and their analysis and conversion into design limits.

1. Introduction

The objectives of the current fusion technology programme can be divided into three types of reactor: (1) an International Thermonuclear Experimental Reactor (ITER), (2) a DEMOnstration reactor (DEMO) and (3) a Commercial Fusion Reactor (CFR). From the structural materials point of view, ITER is a low temperature reactor (<300°C); its main technical objectives are to demonstrate controlled ignition and extended burn. DEMO is an elevated temperature reactor (EU design 250–550°C); it extends the ITER objectives to include sustained burn and tritium breeding. CFR, would very likely be an even higher temperature reactor ($\geqslant$ 550°C); it is intended as a viable alternative to the present commercial fission reactors. All these reactors have a common major obstacle in their development, i.e. the availability of materials to resist the severe thermo-mechanical loadings and irradiation damage encountered in the fusion reactors.

It is, therefore, not surprising to note, that, a major part of the fusion R&D work has focused on the development of new materials or characterisation of existing materials for fusion environment. It is also not surprising to note the diversity of materials and manufacturing techniques needed to satisfy demands of various fusion reactor components [1].

In this paper we discuss some of the materials properties data generated for ITER and DEMO and give examples of how these are converted into design limits.

2. Materials

Three types of materials are considered.

- Stainless steel type 316LN-IG, used in the structural components of ITER (vacuum vessel, back-plate, manifolds, shield, divertor cassette body,...) [2].
- One of the two copper alloys, DS-copper and CuCrZr, envisaged for high heat flux components of ITER (first wall and divertor) [3].
- Martensitic steel type Modified 9Cr–1Mo [4], low activation grades [5] of which are developed for the structural components of DEMO.

Table 1 gives the chemical compositions of these alloys. Notice that the type 316LN-IG steel is similar to the nuclear grades of 316LN steel specified in US and Japan, and in particular in Europe to the steel Z2 CND 17-12 with controlled nitrogen addition, see RCC-MR [6]. This similarity allows us to use the information available in these codes and, hence, considerably reduce the work needed for qualification of this steel for fusion

* Corresponding author.

0022-3115/98/$19.00
PII: S0022-3115(98)00080-4

Table 1
Chemical compositions (wt.%) of the three materials discussed in this paper

wt.%	316LN-IG	9Cr-Mo	CuCrZr-IG
C	0.015–0.030	0.080–0.120	
Mn	1.6–2.0	0.30–0.50	
Si	<0.50	0.20–0.50	(0.011)
P	<0.025	<0.020	$\leqslant 0.04$
S	0.005–0.01	<0.010	(0.0023)
Cr	17.0–18.0	8.00–9.00	0.65–0.80
Ni	12.0–12.5	<0.20	
Mo	2.30–2.70	0.85–1.05	
Al		<0.040	
Fe	Bal.	Bal.	(0.010)
Nb + Ta + Ti	<0.15	0.06 < Nb < 0.10	
V		0.17–0.25	
Cu	<0.3	<0.10	Bal.
Zr			0.07–0.15
O_2			(0.0020)
B	<0.0020		
Co [1]	<0.25		(0.06)
N_2	0.060–0.080	0.030–0.070	

[1] In irradiated materials less than 0.05%.

reactors. The Modified 9Cr–1Mo steel is also similar to the same grade steels used in US, Japan, and Europe, see Z10 CDVNb 9.1 in RCC-MR [6] and Grade 91 in ASME [7]. The equivalent grades of this steel envisaged for DEMO, have molybdenum and other high activation elements replaced by their equivalent low activation elements (e.g. W). CuCrZr alloy discussed here, is similar to the alloy used in JET, and currently proposed as an ITER Grade specification [8]. However, unlike the two steels mentioned above, this alloy is not code qualified and its database is relatively poor.

3. General design considerations

Design limits are derived from qualified material databases. That is, the data collected for a given material are first sorted out and then verified against a set of criteria before being integrated in the database. One of the important considerations checked during the above verification is the initial state of the materials. For instance, the data collected on Type 316LN steel are sorted out to retain those relevant to a solution annealed material (30 min at about 1050°C), and a grain size number of 4–6. Likewise, the data on Modified 9Cr–1Mo steel are sorted out to retain those relevant to a quenched and tempered material (for tubes normalisation at >1040°C, and temper at >730°C). In addition, the data generated are further classified according to the product sizes and shapes. These verifications are particularly important for materials such as Modified 9Cr–1Mo steel and CuCrZr alloy (30 min at 980°C, 50–90% C.W., 4 h at 450°C) that rely on tightly defined thermo-mechanical treatments to achieve their optimum properties. Also to be noted is, that, the safety factors included in the design codes are for such materials, and only cover eventual degradations of materials with such initial properties during a given service condition.

While it is admitted that some of the fabrication procedures envisaged for fusion reactors components will significantly affect the initial materials properties [1] [9–12], we assume that these processes will be sufficiently optimised in time, in a way that the properties of the stainless steel and the martensitic steel will remain within their original specifications. In the case of CuCrZr, knowing that it would be practically impossible to cold work these alloys after their joining to steel, whenever possible, we shall use the data generated on materials in the quenched and aged condition (980°C + 4 h at 450°C).

For simplicity and space, the discussion is limited to the unirradiated properties. The reader is referred to ITER ISDC reports for work on irradiation effects [13]. The external data sources used in this paper are mainly RCC-MR [6], ITER ISDC [13] and ITER MPH [8].

[1] This is particulatly true for the in vessel components, where advanced fabrication techniques, such as Hot Isostatic Pressing, are envisaged for fabrication of single and multilayered components. These techniques usually involve holding the material at very high temperatures (1000–1100°C) for relatively long periods. As a result, the initial materials properties could significantly change.

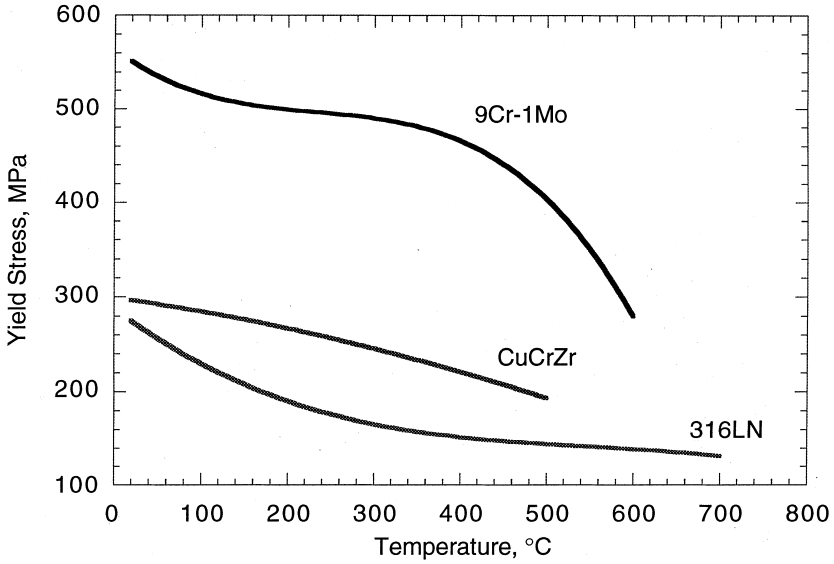

Fig. 1. Average yield stress versus temperature trend curves for stainless steel, martensitic steel and copper alloy.

4. Tensile properties

The allowable primary membrane stress intensity is designated as S_m and is deduced from the following tensile properties.

- The 0.2% offset yield stress obtained in an uniaxial tension test at a given strain rate, R_p or S_y.
- The engineering stress at the point of maximum load in a uniaxial tension test at a given strain rate, R_m or S_u.

4.1. Average tensile properties

Fig. 1 shows plots of the average S_y versus temperature for the three materials. [2] Equations representing these plots are:

$$\text{316LN:}\quad S_{y\ 0.2\ \text{average}} = 275(1.0453 - 2.5053\times10^{-3}\theta + 4.1763\times10^{-6}\theta^2 - 2.5069\times10^{-9}\theta^3)$$

(min. curve is obtained by replacing 275 with 220 MPa).

$$\text{Mod. 9Cr–1Mo:}\quad S_{y\ \text{average}} = 564.25 - 0.7108\theta + 2.6894\times10^{-3}\theta^2 - 3.8267\times10^{-6}\theta^3$$

(min. curve is obtained by multiplying the above equation with 0.7)

$$\text{CuCrZr:}\quad S_{y\ \text{average}} = 299.9 - 0.1286\ \theta - 1.673\times10^{-4}\ \theta^2,$$

$$S_y(\text{min.}) = 267 - 0.12215\ \theta - 1.842\times10^{-4}\ \theta^2.$$

Notice, that both CuCrZr alloy and Mod. 9Cr–1Mo steel show a higher yield strength than 316LN steel, at least at temperatures up to 500°C. However, the strength of these materials sharply declines at higher temperatures. In fact, Mod. 9Cr–1Mo steel is seldom used at temperatures above 600°C. CuCrZr is also not recommended for prolonged service at high temperatures (>300°C) due to the risk of overageing.

Fig. 2 shows plots of the S_u versus temperature for the three materials, where it can be seen that the position of 316LN has improved as compared with Fig. 1. [3]

4.2. Minimum tensile properties

Minimum properties are derived from the scatter band of data around the average values. In the ITER ISDC, the procedures used for calculating min. values of stainless steel (and here extended to 9 Cr steel) are based on the RCC-MR and ASME recommended methods:

$$S_{(\theta\ \text{min.})} = S_{(\theta\ \text{average})}\left(S_{(\text{specified at } 20)}/S_{(\text{average at } 20)}\right),$$

where S_θ represents strength at temperature and S_{20} strength at 20°C.

[2] Martensitic steel plots shown here, are for thick tubeplates, for thin sections and steam generator tubes, higher values are specified at temperatures less than 100°C.

[3] Notice that the difference between S_y and S_u of 316LN-IG is a good indication of its work hardening capability and hence its excellent toughness.

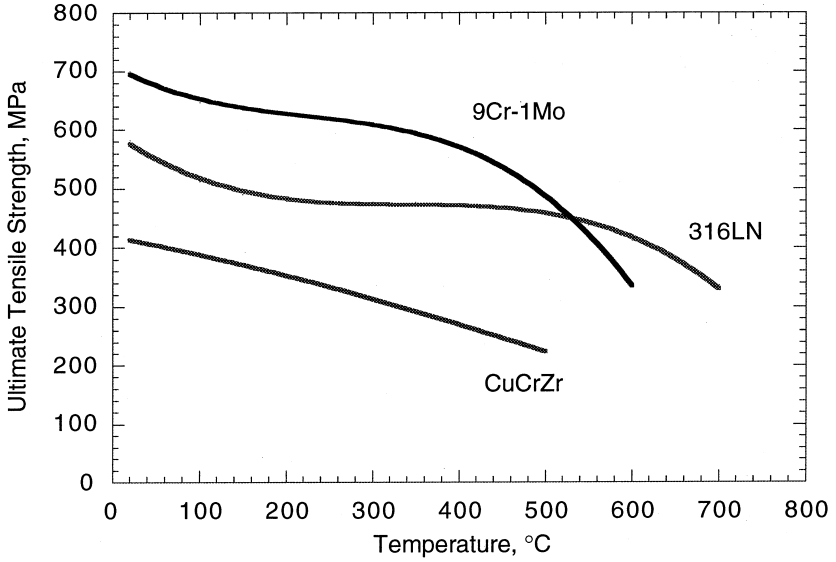

Fig. 2. Average ultimate tensile strength versus temperature trend curves for stainless steel, martensitic steel and copper alloy.

Specified values at room temperature are generally equal to the min. values calculated at room temperature, that here are equal to the average value minus 1.96 × (standard deviation), [4] or a confidence level of 97.5% that the data will be above the min. values.

The databases for 316LN and 9Cr steel are fairly good and the minimum values are derived with adequate accuracy. In contrast, the database for the copper alloys is poor and the minimum values calculated are tentative values.

4.3. S_m

S_m is a temperature (θ) dependent allowable stress intensity defined in RCC-MR as the least of the quantities shown in Table 2.

Copper alloys would qualify as "other" in this table and hence subjected to more severe safety coefficients, unless one can proceed with design by analyses. The differences between the two treatments are very important, as in others, the allowable design stresses for CuCrZr would fall below 100 MPa.

Fig. 3 shows plots of S_m versus temperature for the three materials. S_m is governed by the yield stress of 316LN steel and by the S_m of 9Cr–1Mo and CuCrZr ($\frac{1}{3}$ coefficient).

[4] Where more appropriate, we have used the standard deviation and the average value at a given temperature for calculation of minimum curves. For instance, we have noted that the data of 316LN are sometimes better bound by the min. curve obtained from min. values at 550°C.

5. Creep properties

Time dependent design limits are derived from the creep properties. These limits have received less attention so far in ITER, due to the fact that ITER will be operating at low temperatures (<300°C). At such temperatures stainless steel is in the negligible thermal creep region. In contrast, copper and copper alloys will be in the thermal creep region. DEMO and CFR operating temperatures are considerably higher and, therefore, time dependent properties will play a major role in their design.

In Sections 5.1–5.3, we present a few examples of the procedures used to calculate the time dependent design limits.

5.1. Creep rupture

Creep rupture data are used to determine S_r values (minimum stress to cause rupture in a given time at a given temperature). For this purpose, stress rupture values are plotted versus an equivalent time–temperature parameter, e.g. the Larson–Miller parameter ($P = (\theta + 273)(\log t + C)$, and fitted with an average trend

Table 2
Coefficients used in RCC-MR for austenitic, ferritic-martensitic steels and other alloys

	$S_{y\ \text{min. } 20°C}$ (specified)	$S_{y\ \text{min. } (\theta)}$	$S_{u\ \text{min. } 20°C}$ (specified)	$S_{u\ \text{min. } (\theta)}$
316LN	2/3	0.9	1/3	1/2.7
9Cr–1Mo	2/3	2/3	1/3	1/3
Others	2/3	2/3	1/4	1/4

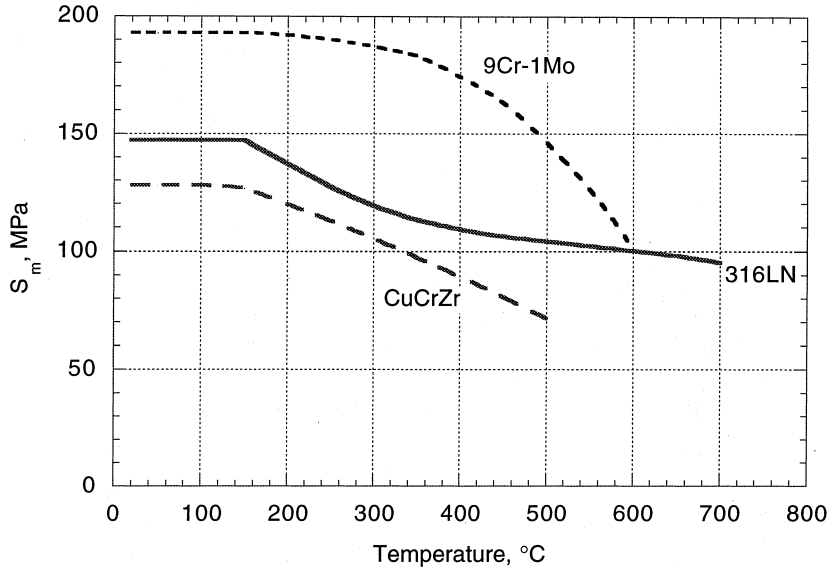

Fig. 3. S_m versus temperature.

curve. The constant C is separately calculated for best fit. The minimum creep rupture curve is obtained by subtracting 1.96 SD from the average curve.

Fig. 4 shows an example of the master creep rupture curve obtained for the Mod. 9Cr–1Mo steel. The minimum creep rupture curve is also plotted in the same figure. From the minimum curve, values of S_r for various times and temperatures can be calculated and tabulated. Similar curves are also available for the austenitic stainless steel, but the database for CuCrZr alloy is very poor.

5.2. Isochronous curves

Isochronous curves are used in design to limit combined deformations due to tension and creep.

$\varepsilon_t = \varepsilon_e + \varepsilon_p + \varepsilon_c$.

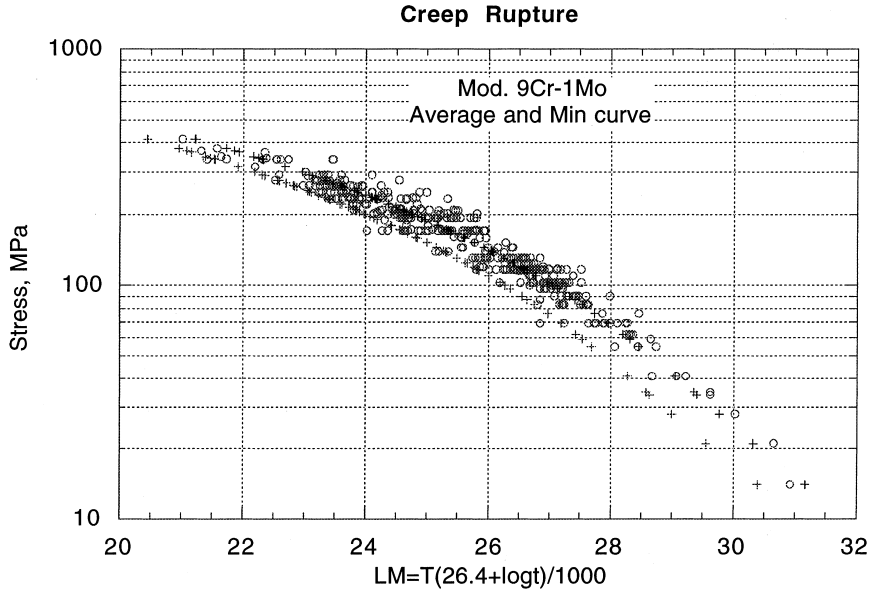

Fig. 4. Master plot for deriving S_r values of Mod. 9Cr–1Mo.

In this equation, tensile strain is represented by the sum of elastic (ε_e) and plastic (ε_p) strains, and creep strain by (ε_c).

The elastic strain is calculated from $\varepsilon_e = \sigma/E$, where values of the Young's modulus (MPa) are calculated from its variation versus temperature (°C):

$$E = \begin{cases} 194\,000 - 81.4\theta & \text{for 316LN} \\ 207\,300 - 64.58\theta & \text{for 9Cr–1Mo steel} \\ & 20 \leqslant \theta \leqslant 500 \\ 295\,000 - 240\theta & \text{for 9Cr–1Mo steel} \\ & 500 \leqslant \theta \leqslant 600 \\ 129.2039 - 3.4523 & \\ \times 10^{-2}\theta - 4.1233 \times 10^{-5}\theta^2 & \text{for CuCrZr} \end{cases}$$

The plastic component of the tension curve is derived from the work hardening equation. One way of doing this, is to plot the normalised values of the yield stress ($S_y^{(\theta)}/S_{y\ 0.2}$) versus plastic deformation on a log–log scale and fit a power law curve to the data.

The equation for 316LN has the following form:

$$\sigma_{\text{average}} = S_{y\ 0.2\ \text{average}} \times 1.17\varepsilon_p^{0.096}.$$

This equation is valid between 0.001% and 1%.

An example of the average curves obtained with this equation is shown in Fig. 5.

The equation for the Modified 9Cr–1Mo steel is similar. However, unlike 316LN, values of C and n vary with temperature for the Mod. 9Cr–1Mo steel.

The creep component of the isochronous curves is calculated from the creep curve (primary plus secondary creep).

If the service temperature is below the creep regime, then, there is no creep, $\varepsilon_c = 0$, and the minimum tension curves represent the isochronous curves. This is the case of 316LN in ITER. If the temperature is greater than the negligible creep range (>425°C), then, deformations resulting from the primary and the secondary creep are added, unless the primary creep is indefinite (this is the case of stainless steel at temperatures between 425°C and 480°C).

Various coefficients and exponents are tabulated in RCC-MR tables. Minimum isochronous curves are obtained by using the min. tension curves instead of the average curves. In general, however, a factor of 0.8 is applied to the average curves to obtain the min. curves. Fig. 6 shows plots of isochronous curves obtained for the Mod. 9Cr–1Mo steel at 550°C.

5.3. Design criteria S_t and S_{mt}

S_t is a design criterion derived from three conditions:

- $\frac{2}{3}S_r\ (\theta, t)$
- 80% of min. stress to the end of secondary stage in time t
- Stress from the min. isochronous curve that results in 1% deformation (elastic + plastic + creep).

Combining the limits of S_m and S_t and choosing the minimum of the two, gives S_{mt}. Fig. 7 shows an example of this for the 9Cr-lMo steel.

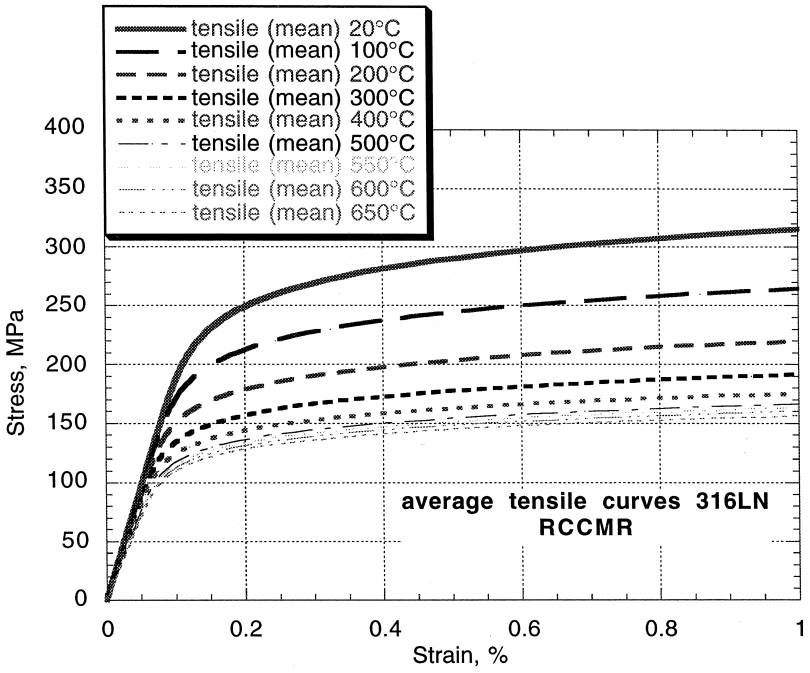

Fig. 5. Average tension curves of 316LN at temperatures 20–650°C.

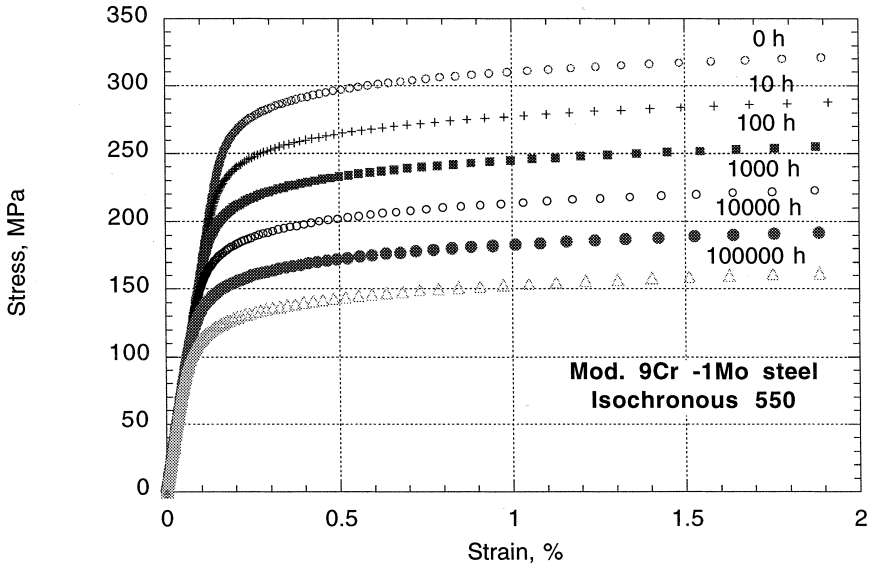

Fig. 6. Average isochronous curves of Mod. 9Cr–1Mo steel at 550°C.

6. Fatigue and fatigue–creep properties

Damage resulting from repeated loading is controlled through fatigue design limits. For this purpose continuous fatigue and fatigue–creep tests are performed on appropriate specimens. [5] Two types of test are generally performed, (a) strain controlled and (b) load controlled tests, with the former being more relevant to fusion reactors (low cycle fatigue, thermal stresses). Most of these tests are performed using fully reversible triangular cycles at a strain rate of about 3×10^{-3}/s.

Fig. 8 shows an schematic representation of the variations of strain and stress versus time, during a continuous fatigue test and a simultaneous fatigue–creep test. [6] In the latter case, the specimen is held at max. tension and/or compression side of the fatigue cycle for a given time (Δt). During this hold period, stress relaxation occurs while the deformation remains constant.

6.1. Continuous fatigue

Fig. 9 shows plots of the fatigue endurance for the three materials. Those of the 316LN and the Mod. 9Cr–1Mo steels are at 550°C and the one for CuCrZr at 350°C. Additional data on CuCrZr have been reported in [14–17] but, here, only data given in IMPH are used. For comparison, it is pointed out that the fatigue endurance curves of the two steels at 350°C are slightly higher than the curves shown at 550°C.

The average curves are fitted in Fig. 9 using the Langer equation in order to account for the fatigue threshold at high cycles. In the low cycle region, Manson–Coffin equations (strain range partitioning) can also be used with adequate accuracy. Design curves are obtained from the average curves by applying a factor of 2 to the strain range and 20 to the number of cycles to rupture.

6.2. Cyclic hardening curves

These curves are used, amongst others, to calculate creep damage in creep–fatigue tests. The usual procedure is to plot half stress range, taken at half life [7],

[5] Unlike tensile and creep properties, fatigue test results are very sensitive to specimen shape, specimen preparation, testing conditions, extensometry, etc. The data used for code analyses are, therefore, rigourously controlled with respect to these parameters. For instance, in the case of 316LN and 9Cr-1Mo steels, the data are sorted to retain only those obtained on standard parallel sided specimens (no miniaturised or hourglass specimens) with axial extensometry. Fatigue data collected on copper alloys come from various laboratories and have yet to be fully validated.

[6] As compared with the simultaneous fatigue–creep testing, sequential fatigue–creep or creep–fatigue testing consists of fatigue cycling the specimen for a number of times before subjecting it to creep (or vice versa). Fatigue and creep loading parameters are varied to cover different combinations.

[7] By convention half life value is used. However, not all the materials show typical plateau observed for SS after initial rapid hardening during a test. Martensitic and copper alloys could even show a fatigue softening.

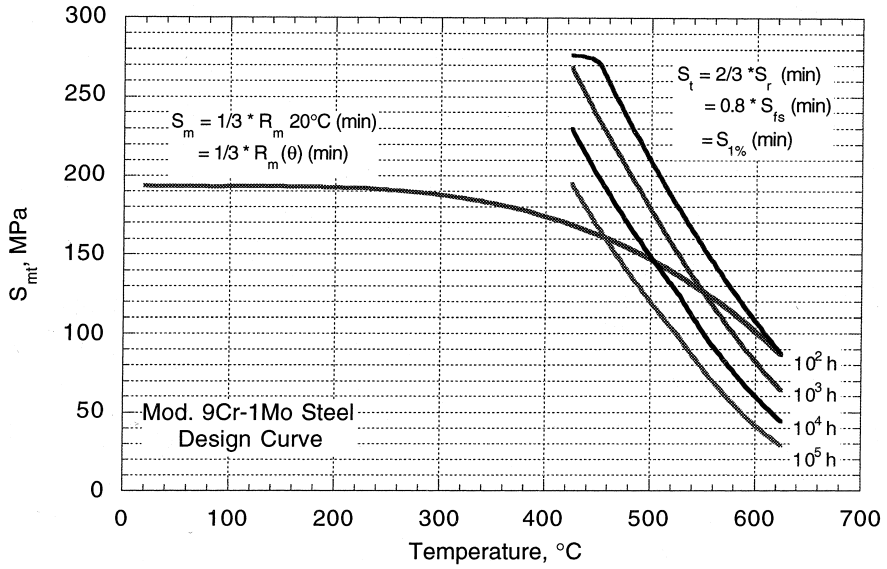

Fig. 7. Determination of S_{mt} for Mod. 9Cr–1Mo steel.

versus half strain range, to obtain a similar plot as those obtained from tension tests. The initial strain at first quarter cycle is often used to plot the latter (monotonic hardening). This method has the advantage of using data from the same material for both monotonic and cyclic hardening curves. Equations describing cyclic hardening of 316LN and Mod. 9Cr–1Mo steel have been presented elsewhere [2,4]. Fig. 10 presents these curves for CuCrZr alloy (data extracted from [14]).

6.3. Fatigue–creep damage calculation

Fatigue–creep interaction occurs when the material is subjected to the two types of loadings. The operating mode of ITER is a good example of this. There, fatigue damage is due to heating ups and cooling downs, and the creep damage due to the sum of pulse durations ($\Delta t = 1000$ s). In ITER, fatigue damage is the dominant parameter, as the first wall will be subjected to several

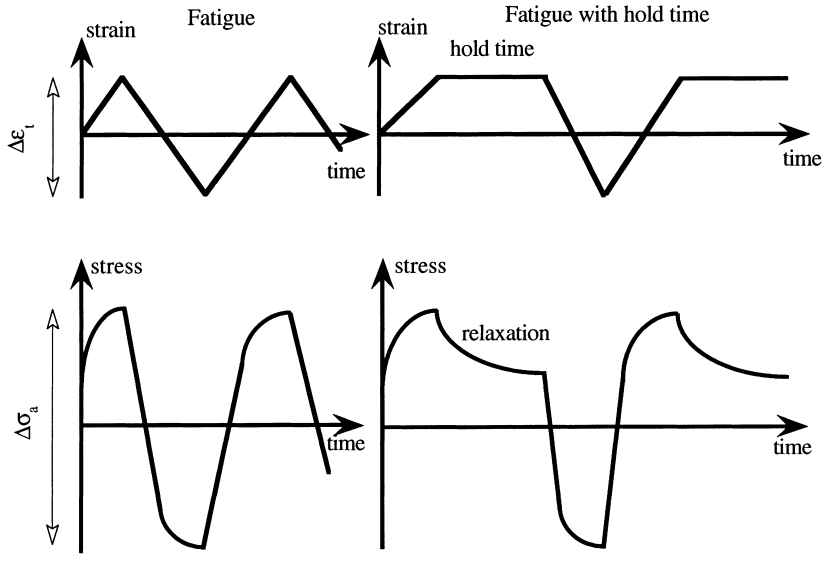

Fig. 8. Schematic representation of the evolutions of strain and stress versus time, in strain controlled continuous fatigue and creep–fatigue tests.

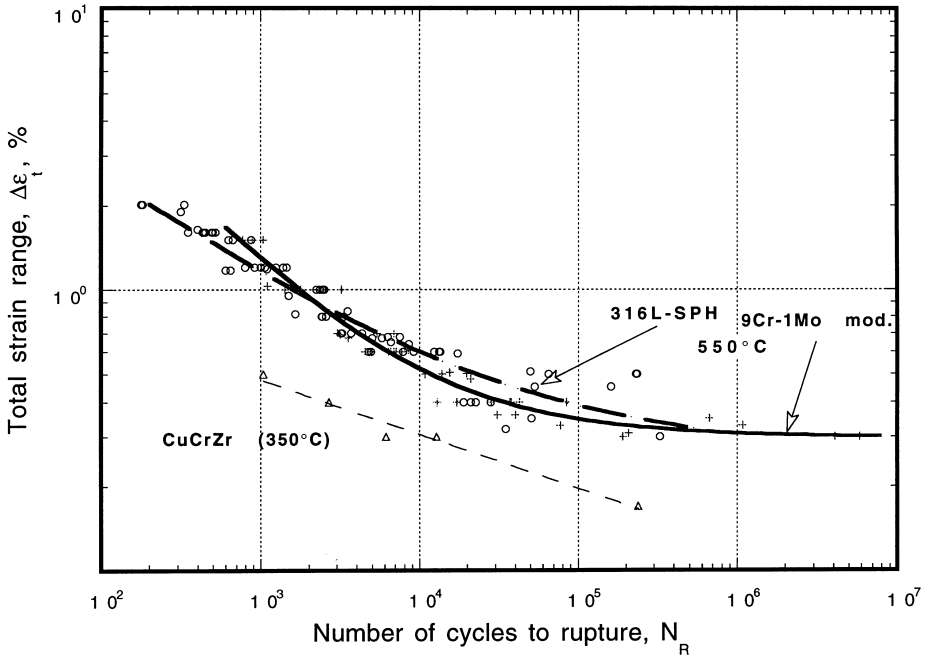

Fig. 9. Comparison of fatigue database at one temperature for three alloys.

thousand short exposures. In DEMO and CFR, the reactor will be operating for long intervals (>100 h) before it is shut down. As a result, the creep component of the creep–fatigue damage will be greater.

Two methods are used for calculating fatigue–creep damage. One is time based and the other ductility based. The simplest one to use is time based linear damage cumulation. Here, the fatigue part of the damage (N/N_f) is calculated from the ratio of the number of cycles (N) over the number of cycles to rupture under the same strain range in continuous fatigue (N_f). The creep part of the damage (t/t_r) is calculated by adding the time of hold times at a given stress (calculated from cyclic hardening curves) and dividing it by the time to rupture at the same

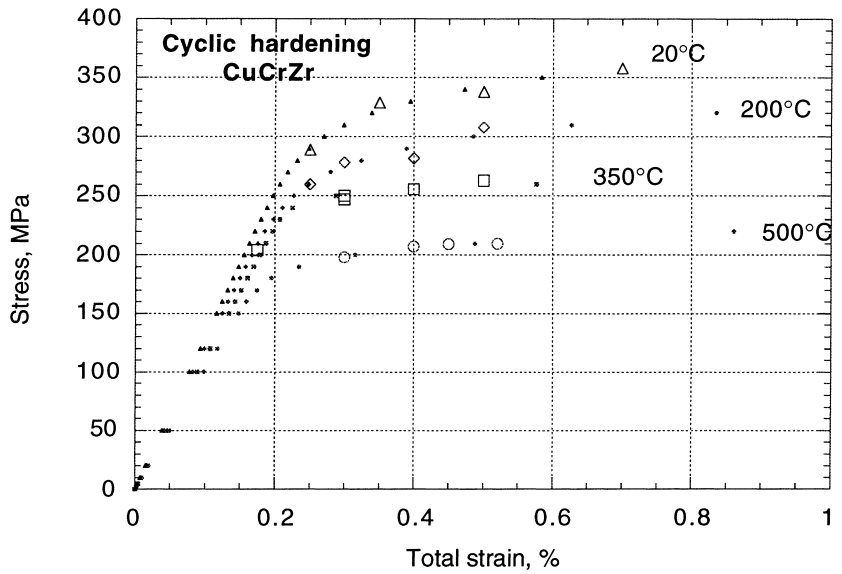

Fig. 10. Calculated cyclic hardening curves for CuCrZr alloy shown with experimental data (larger captions).

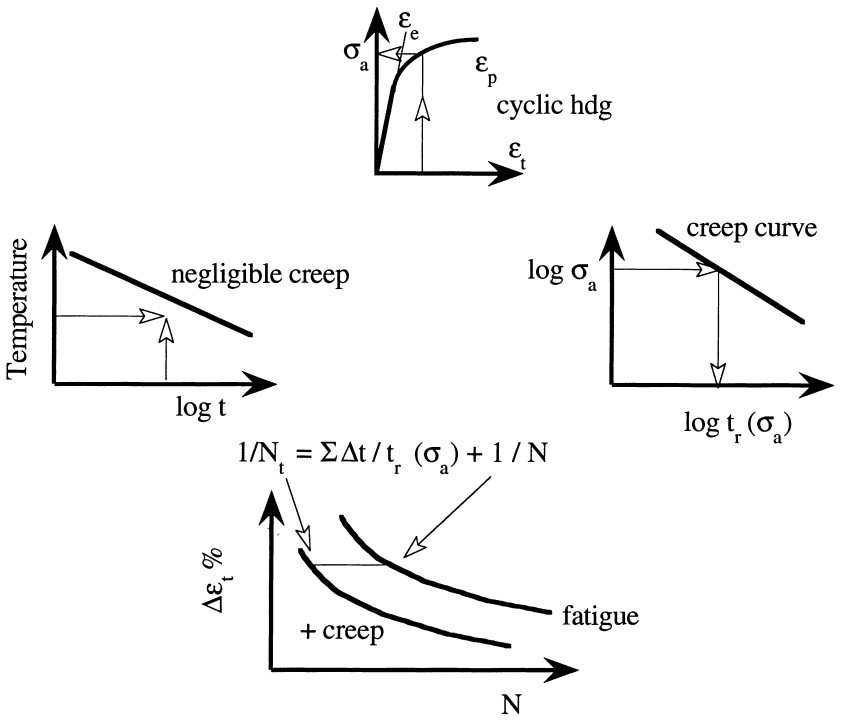

Fig. 11. Schematic representation of creep–fatigue damage calculation.

stress in continuous creep. If creep is negligible, then fatigue design curve remains unchanged. If the creep damage is not negligible, then the outcome would result in a shift of the fatigue design curve, Fig. 11.

The actual calculation, however, is not so simple. This is due to the fact that the peak stress at which hold time starts varies during a fatigue test, and that different relaxation curves could result from this. An approximate solution is to use the stress at half life, fit a curve to the relaxation data at this stress, and then use this curve as the reference curve for all cycles. The relaxation curve is divided into several segments and an average stress is calculated for each segment and used to calculate the creep damage per segment [18], Fig. 12.

6.4. Fatigue–creep interaction diagram

Calculated creep and fatigue damage fractions are plotted on an interaction diagram, where pure creep damage is represented by coordinates (0,1), and pure fatigue damage by coordinates (1,0). In ASME and RCC-MR, these points are connected to a point with coordinates (0.3; 0.3) for stainless steel. The cumulated damage must lie below this limit to avoid failure.

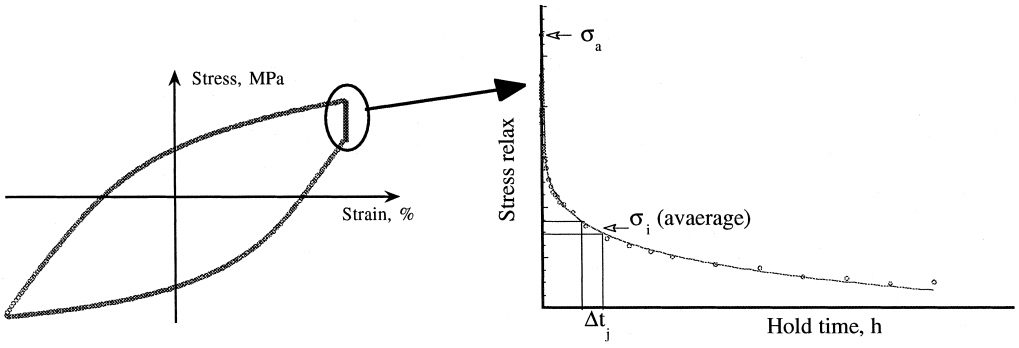

Fig. 12. Example of the curve fitted to the 9Cr–1Mo relaxation curve.

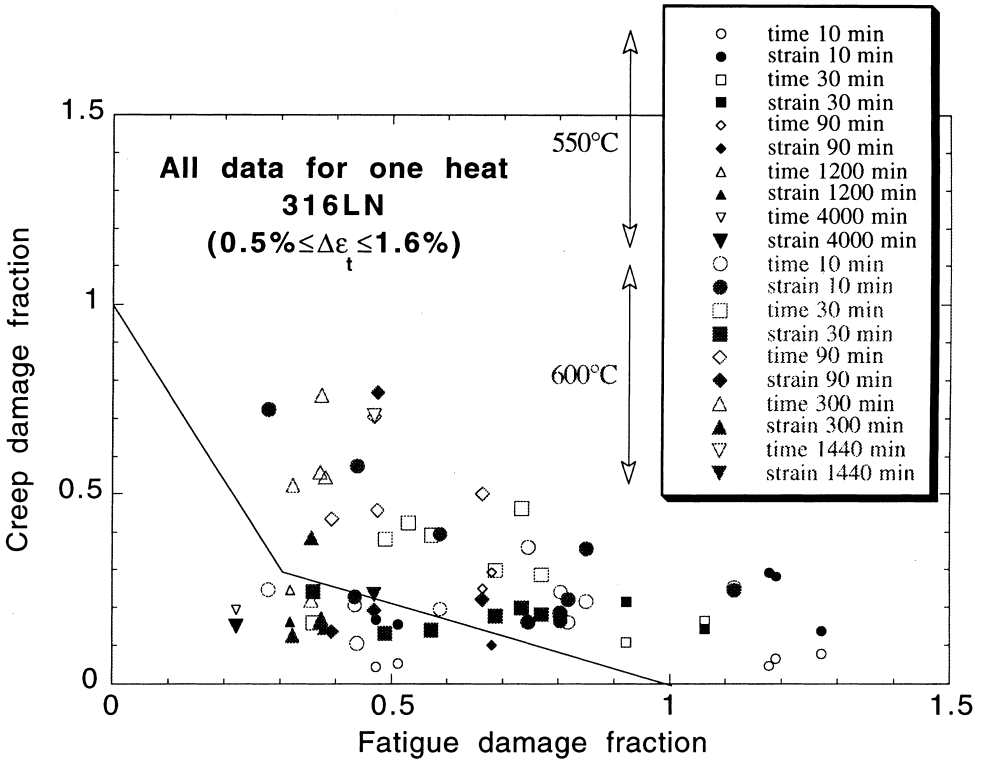

Fig. 13. Example of fatigue–creep test results obtained for 316LN. Experimental results shown in this figure are limited to one heat and to code qualified results.

As shown in Fig. 13, neither method of damage calculation is perfect [19]. Often, cumulated damage before failure is far greater than 1, suggesting an over-conservatism of design. This is due to the fact that one damage mechanism can clear the damage from the previous mechanism by rearranging the dislocation substructure. However, there are cases where failures are below the experimental data available. Since, creep–fatigue tests are very long tests, there is a tendency to accelerate these tests by applying high strain ranges. The results obtained from such tests are seldom applicable to the lower strain range tests.

7. Conclusions

- Existing codes and procedures can be used to calculate most of the design criteria needed for fusion reactors.
- Additional design Criteria are being written for ITER and DEMO to include effects not covered by the existing rules (e.g. effects of irradiation).
- Full adaptation of either set of rules for fusion reactors is, nevertheless, hindered due to utilisation of high temperature manufacturing techniques that could alter the initial materials properties or the lack of data for some materials.

References

[1] A.A. Tavassoli, Overview of Advanced Techniques for Fabrication and Testing of ITER Multilayer Plasma Facing Walls, ISFNT-4, Tokyo, 6–11 April 1997.
[2] A.A. Tavassoli, Assessment of austenitic stainless steels, Fusion Eng. and Design 29 (1995) 371–390; Proceeding of Int. Symposium on Fusion Nuclear Technology-3, 26 June–1 July 1994, UCLA, Cal., Fusion Eng. and Design 29 (1995) 371–390.
[3] G. Kalinin, W. Gauster, R. Matera, A-A. Tavassoli, A. Rowcliffe, S. Fabrietsiev, H. Kawamura, Structural materials for ITER in-vessel component design, Invited Paper, International Conference on Fusion Reactor Materials-7, Obninsk, F.R., 25–29 September 1995, JMN 11283, 1996.
[4] J.W. Wareing, A.-A. Tavassoli, in: S.V. Möller, J.D. Riera (Eds.), Structural Problems of Fast Reactors and other Types of Reactors, Transactions of the 13th International Conference on Structural Mechanics in Reactor Technology, Porte Alegre, Brazil, Aug. 1995, p. 563.
[5] A. Hishinuma, A. Kohyama, R.L. Klueh, D.S. Gelles, W. Dietz, K. Ehrlich, these Proceedings.

[6] RCC-MR Règles de Conception et de Construction des Matériels Mécaniques des Ilots Nucléaires RNR., tomes I et II, AFCEN, édition 1993.
[7] ASME Boiler and Pressure Vessel Code, Section III, Case N47-14, (Class I components in Elevated temperature service.), American Society of Mechanical Engineers, Nea York, 1978, p. 105.
[8] ITER Materials Properties Handbook, prepared by ITER partners, Package 3, August 1997.
[9] H. Takatsu, Status of T212: Cu/SS joining techniques development and testing, Blanket Working meeting, Garching, 19–23 February 1996.
[10] M. Fèbvre et al., Solid HIPed Demonstrator of ITER Blanket-shield modules, SOFT-19, Lisbon, 16–20 September 1996.
[11] K.T. Slattery, D.E. Driemeyer, G.D. Morgan, G.W. Wille, Development of 316LN-IG stainless steel fabrication approaches for ITER Divertor and Limiter applications, FW-P43, ISFNT-4, Tokyo, Japan, 6–11 April 1997.
[12] E. van Osch, ITER Task T214, ECN report on 2 dpa irradiation at 325°C, presented by A.-A. Tavassoli at ITER Garching JWS, 12 November 1996.
[13] ITER Interim Structural Design Criteria, prepared by ITER partners, 6th edition, August 1997.
[14] K. Leedy, PhD thesis, University of Illinois at Urbana-Champaign, 1997.
[15] D.J. Edwards, B.N. Singh, O. Toft, K. Morita, these Proceedings.
[16] G. Le Marois et al., ISFNT-4, Tokyo, Japan, 6–11 April 1997.
[17] S.A. Fabrietsiev, Status and Progress Report on Copper Alloys and Joints Irradiation, ITER Working meeting, Garching, 24–26 March 1997.
[18] I. Bretherton, A.A. Tavassoli, M. Mottot, Fatigue and creep-fatigue failure in wrought modified 9Cr 1Mo ferritic steel, CEC contract RA1-CT94-0241-UK, March 1994.
[19] H. Breitling, E. Stärk, V.B. Livesey, M. Mottot, A.-A. Tavassoli, Evaluation of Creep-Fatigue Behaviour of Austenitic Stainless Steels, Structural Mechanics In Reactor Technology (SMIRT-12), BG12/2, Stuttgart, 15-20/08/93.